Mobile Networks and Applications (2021) 26:1960–1970
https://doi.org/10.1007/s11036-020-01728-8

Research on Image Fusion Algorithm Based on NSST Frequency Division and Improved LSCN

Hongna Zhang [1] · Wei Yan [2] · Chunyou Zhang [1] · Lihua Wang [1]

Accepted: 6 December 2020 / Published online: 3 January 2021

Abstract
Single modal medical images provide limited information and cannot reflect all the details of the relevant tissues, which may lead to misdiagnosis in clinical medicine. Therefore, a medical image fusion algorithm based on non-down-sampling shear wave transform (NSST) is proposed. This algorithm fuses multi-modal medical images, enriches the information of fused images, improves the image quality, and provides a basis for clinical diagnosis. Firstly, the low-frequency sub-band and several high-frequency directional sub-bands are obtained by NSST transformation of the source image, and the structural similarity between sub-bands is evaluated. Then, according to the characteristics of low-frequency sub-band images, for sub-images with high similarity, the regional features are obtained by region energy and variance, and the fusion method is based on region feature weighting. For sub-images with low similarity, two images to be fused are input into the LSCN model respectively by fusing the connection items of the improved LSCN model. The improved L-term replaces the ignition frequency in the traditional PCNN as the output. According to the characteristics of high frequency sub-images, the fusion rule of combining visual sensitivity coefficient and regional energy is adopted for sub-images with high similarity. For sub-images with low similarity, an improved guided filter is used to fuse the sub-images in order to maintain the clear edges of the images. Finally, the image is reconstructed by inverse NSST transform. The experimental results show that the proposed algorithm can obtain better fusion effects in both objective and subjective evaluation. The obtained fusion image has rich information, excellent edge retention characteristics, subjectively clear texture and high contrast and good visual effect.

Keywords NSST frequency division · Medical image fusion · Non-subsampled Shearlet Transtransform · Structural similarity evaluation between sub-bands · Improved guided filter

1 Introduction

With the continuous development of science and technology, there are many types of medical images for reference in clinical diagnosis. The information of human tissues and organs can be reflected in different modal medical images [1]. High-density tissues can be observed by computed tomography (CT) images, and soft tissue is not suitable for CT image observation. Magnetic resonance imaging (MRI) cannot express dynamic information, but it has high resolution in soft tissue image detection and recognition and can present details in multiple angles and multiple planes [2]. Single-photon emission computed tomography (SPECT) can achieve low resolution, but can provide sensitive image information of organs and tissues [1]. This indicates that although single-modal images have unique advantages in representing characteristic information of human tissues, single-modal images often fail to provide sufficient information for doctors to diagnose diseases. Therefore, medical images need multimodal fusion to compensate for the lack of information in a single mode. That is to say, salient features and important information from multiple different modal medical images are fused into one image, which can better show the texture contour of the source image. The fusion image information is more abundant, which improves the effectiveness of image diagnosis.

Image fusion maximizes the retention of detailed features while preserving the information of the source image [3].

✉ Hongna Zhang
zhnimun@163.com

✉ Wei Yan
wei.yan@ufl.edu

[1] College of Mechanical Engineering, Inner Mongolia University for the Nationalities, Tongliao 028000, China

[2] College of Mechanical Engineering, University of Florida, Gainesville, FL 32611, USA

Multi-scale decomposition is widely used in medical image fusion because of its obvious advantages in obtaining effective feature information. Villadsen et al. proposed a contrast pyramid image fusion scheme [4]. In this scheme, the source image is decomposed into several expression layers, each of which is correlated with the contrast in frequency. This method can represent image feature information at multi-scale and multi-resolution. This method can reflect image information at multiple scales and high resolutions, but the interference between redundant decomposition and decomposition variables [5]. Huang et al. [6] proposed a differential evolution image fusion technique. This method uses wavelet transform to process the source object, and then optimizes it according to the differential evolution objective function. The problem is that the image spectrum is distorted after fusion. Li et al. proposed a medical image fusion algorithm based on lifting wavelet transform, but the effect is not ideal in the detail processing of texture edges [7]. Vishwakarma et al. found that Contourlet transform theory can make up for the defects of wavelet transform, and proposed an image fusion method based on Contourlet transform weighting coefficient [8].Huang et al. found that the Contourlet transform theory can effectively fuse multi-source medical images, but it does not get the edge features of the images. After in-depth study, Huang et al. A fusion algorithm based on NSST and morphological component analysis (MCA) is proposed [9].Ouerghi et al. obtained a good fusion effect using the NSST-based medical image fusion algorithm [10]. The signal shape and processing mechanism obtained by Eckhorn through pulse coupled neural network (PCNN) is more in line with the physiological characteristics of the human visual nervous system due to the simplified artificial neural network [11]. Ganasala et al. found that the PCNN network model is simple, and has obvious advantages in image fusion, image segmentation and image recognition. A fusion algorithm based on pulse neural coupling network and NSST is proposed [12]. The selection of high frequency and low frequency coefficients is based on the rule that the ignition number of ignition maps is larger. The high frequency coefficients are used as external excitations of the PCNN without regard to the effects of noise, and the characteristics of the image are determined by the corresponding regions, which are difficult to reflect by a single pixel. Cheng et al. combined a multi-scale decomposition algorithm and neural network model to propose a medical image fusion algorithm based on human visual features and adaptive PCNN [13]. However, the contour wave transform greatly reduces the efficiency of the algorithm. Zhao Dan et al. proposed a fusion algorithm combining NSST and PCNN [14]. However, the low-frequency sub-band images are fused by weighted coefficients, which will cause the fuzziness of detail information to a certain extent. Guided filter is a kind of edge-preserving smoothing filter proposed in recent years [15, 16]. The steering filter has the advantages of obvious denoising, smooth detail and good edge preservation. It is widely used in image denoising, image enhancement and image fusion. Zhu et al. proposed a composite shear wave transform (CSWT) fusion method. Improved guidance filtering [17]. Wang proposes a fusion algorithm combining guided filtering and image statistics [18]. Sun G presented the MIC-relevance-average-MIC-redundancy criterion to evaluate the goodness of features, and an approximate Markov-blanket search strategy is then proposed to improve the efficiency of feature selection [19, 20]. Bavirisetti et al. proposed an algorithm that combines NSCT and guided filtering. However, the weight factor of guided filter is constant in this method, which easily leads to the blurring of image details at the edge [20].

This paper mainly studies the fusion of multi-mode medical images,the NSST transform based on the source image combines the low-frequency sub-band image with the improved connector of the LSCN model (L terms) to obtain the low-frequency sub-band and several high-frequency directional sub-bands, the image to be fused is input into the LSCN model and the improved L term is used instead of the ignition frequency in the traditional PCNN as an output. A medical image fusion algorithm based on improved NSST and LSCN is proposed.In order to maintain the clear edge of the image, the improved guided filter of high frequency subgraph is used to fuse. Finally, the image is reconstructed by inverse NSST transform. The experimental results verify the effectiveness of the algorithm.

2 Medical image fusion algorithm

2.1 Basic theory

(1)non- subsampled shearlet transtransform (NSST)

NSST is an improved model of Shearlet. It is mainly used in image denoising, target recognition, defect extraction, image enhancement, image fusion, etc. It has translation invariance, multi-directionality and low computational complexity.The NSST transformation is mainly divided into the following two steps, that is multi-scale decomposition and direction localization. Multi-scale decomposition is implemented by non-sub-amplified Laplacian pyr-amid (NSLP) to ensure translation invariance and suppress pseudo-Gibbs phenomenon. Direction localization is achieved by a shear filter (SF). The source image is decomposed by n stages to obtain 1 low frequency sub-band image and n high frequency sub-band images of the same size but different scales. The level 3 NSST decomposition decomposition process is shown in Fig. 1.

It can be seen from the structure of the NSCT that, the source image is decomposed into a low frequency sub-band and l high frequency sub-band after the NSST l level transformation, and among them, among them, the non-downsampling direction filter group decomposes the high-

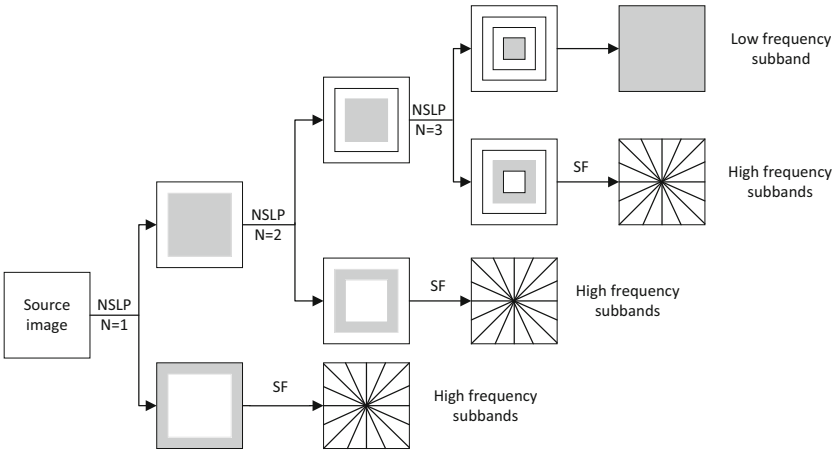

Fig. 1 NSST multi-scale multi-directional decomposition process

frequency sub-bands of each level in the *k*-level direction, and generates *l* band-pass sub-band image images of the same size as the source image.

(2)LSCN basic structure.

Zhan et al. were inspired by Ecknorn et al. in the design of the model, and in January 2017 proposed the Link Synaptic Computing Network (LSCN) model [21, 22]. The model can properly describe the exponential decay of bioelectric transmission and the simultaneous transmission of pulses by adjacent neurons when the visual cortex is stimulated. In addition, the model can also use pulse synchronous release phenomena to stimulate and suppress adjacent neurons.

There are two main differences between LSCN and PCNN: the first difference is that the membrane potential is represented by the leakage integrator in the model; the second difference is that the feedback input is represented only by the excitation. The basic PCNN model involves five aspects: feed input, connection input, internal activity, ignition threshold, and pulse output. The improved model LSCN can be simplified into the signal acquisition mechanism. Although the LSCN model has three leakage integrators, as long as a convolution calculation is performed, the time complexity of the LSCN model is greatly reduced compared to the PCNN model with two convolutional integrators with three leakage integrators. In addition, the iterative process of the PCNN model needs to be manually set, and the iterative process of the LSCN model can be automatically stopped.

LSCN continues to simplify the input signal acquisition mechanism, and the total number of parameters to be determined is also greatly reduced. There are three leakage integrators in the traditional PCNN model, which requires two convolution operations. In the LSCN model, there are also three leakage integrators, but only one convolution operation is required. This determines that the time complexity of the LSCN model is lower than that of the traditional model. At the same time, it can be seen that the relationship between internal activity items and external incentives in the model is more direct. Not only that, unlike traditional PCNN, the iteration process of the LSCN model is automatically stopped rather than manually set. In multiple iterations, the operation is more convenient.

The LSCN model has obvious advantages over multiple iterations.

The mathematical expression of the LSCN model is as follows:

$$F_{ij}(n) = s_{ij} \tag{1}$$

$$L_{ij}(n) = lL_{ij}(n-1) + \sum_{pq} W_{ijpq} Y_{pq}(n-1) \tag{2}$$

$$U_{ij}(n) = fU_{ij}(n-1) + S_{ij}\left(1 + \beta L_{ij}(n)\right) \tag{3}$$

$$\Theta_{ij}(n) = \Theta_{ij}(n-1) - \delta + hY_{ij(n-1)} \tag{4}$$

$$Y_{ij}(n) = \begin{cases} 1, & U_{ij}(n) > \Theta_{ij}(n) \\ 0, & otherwise \end{cases} \tag{5}$$

Where, $F_{ij}(n)$ is the feedback input for the neuron; (i, j) is the index of each neuron; S_{ij} carries the stimulus information; $L_{ij}(n)$ is the input for the connection; (p, q) is the adjacent neurons; l is the connection constant; W_{ijpq} is the weight applied to the connected synapse; $Y_{ij}(n-1)$ is the post-synaptic Action potential. In this paper, the membrane potential is represented by the leakage integrator, $U_{ij}(n)$ is the internal activity term, f is the membrane potential decay constant, β is the connection strength; the threshold of the neuron is represented by the leakage integrator, $\Theta_{ij}(n)$ is the ignition threshold; δ it is a small normal number; h is the amplitude adjustment; $Y_{ij}(n)$ is the pulse output.

(3) Guided filtering.

Guided filtering is an image filtering technique based on local linear variations with the characteristics of maintaining edges. The guided filter filters the input image p through the guide image I, and the obtained output image has a texture similar to the guide image. The linear model of the guided filter function output image q and the guide image I in a two-dimensional window is as follows:

$$q_i = a_k l_i + b_k \tag{6}$$

where, $i \in \omega_k$,q_i is the first pixel in the output image; a_k and b_k represents the linear coefficient; ω_k represents the window k centered on the pixel; and the two sides of the function are simultaneously derived: $\nabla q_i = a_k \nabla l_i$, it can be seen that when the leading edge of the leading image I_l appears, the output image q will also appear accordingly. The edge of. The output image$q$ is the image after the image p is removed from texture or noise:

$$q_i = p_i + n_i \tag{7}$$

The solution to the linear coefficient sum can be translated into the optimal problem, ie.the minimum difference between and is obtained:

$$E(a_k, b_k) = \sum_{i\in\omega_k}\left((a_k I_i + b_k - p_i)^2 + \varepsilon a_k^2\right. \tag{8}$$

Solving the value of a_k and b_k using linear regression:

$$a_k = \frac{\frac{1}{|\omega|}\sum_{i\epsilon\omega k}\left(\left(I_i\, p_i - u_k \overline{p}_k\right)\right.}{\sigma_k^2 + \varepsilon}\ 10 \tag{9}$$

$$b_k = \overline{p}_k - a_k u_k (11) \tag{10}$$

Where, u_k and σ_k^2 represent the mean and variance of the window ω_k, respectively, ε is the weighting factor, $|\omega_k|$ represents the number of pixels in the window, $\overline{p}_k$ indicates the mean of p_i with the window ω_k. All of the above are formulas for individual pixels, When processing an image, the sliding window form is generally used. The expression of Eq. (7) can be written as:

$$q_i = \frac{1}{|\omega|}\sum_{i\in\omega_k}\left((a_k I_i + b_k) = \overline{a}_i I_i + \overline{b}_i\right. \tag{11}$$

where, $\overline{a}_i = \frac{1}{|\omega|}\sum_{i\epsilon\omega_k} a_k$ $\overline{b}_i = \frac{1}{|\omega|}\sum_{i\epsilon\omega_k} b_k$

2.2 Image integration basic framework

Four-stage decomposition of multimodal medical images using NSST yields a low frequency subband and four high frequency subbands. According to the characteristics of low frequency subband and high frequency subband, based on the subgraph similarity judgment, the subgraphs with low similarity are respectively fused with improved LSCN and improved guided filtering to obtain the low frequency and high frequency after fusion. Subbands, for high-low frequency subgraphs with high similarity, respectively, using regional feature weighting and visual sensitivity combined with regional energy to merge. Finally, the fusion medical image is obtained by the inverse transformation of NSCT. The specific process can be seen in Figs. 2 and 3. Shown as follows:

2.3 Low frequency image fusion strategy

The low-frequency subgraph contains basic information about the image other than texture and detail, and is the embodiment of the overall outline of the image. The fusion of the coefficients is very important. Traditional methods of, neighborhood energy and regional variance not only reduce image brightness, but also weaken low-brightness edges and sensitivity to noise. Combining existing methods, this section first determines the similarity of low-frequency subgraphs, and then different degrees of similarity. The subgraphs use different fusion strategies.

2.3.1 High similarity low frequency subgraph fusion

The edge and non-edge information of the subgraph are calculated by local energy E and variance D, and a linear combination of E and D is calculated to reflect the region features of the subgraph, and then the similarity of the subgraph is calculated. For the subgraph pixel window with $M \times N$, its associated value is calculated:

$$E_L(x,y) = \sum_{i=-\frac{M-1}{2}}^{i=\frac{M-1}{2}}\sum_{j=-\frac{N-1}{2}}^{j=\frac{N-1}{2}} \omega(i,j) C_L(x+i, y+j)^2 \tag{12}$$

$$D_L(x,y) = \frac{1}{M\times N}\sum_{i=-\frac{M-1}{2}}^{i=\frac{M-1}{2}}\sum_{j=-\frac{N-1}{2}}^{j=\frac{N-1}{2}}\left(C_L(x+i,y+j) - \overline{C}_L(x,y)\right)^2 \tag{13}$$

$$M_L(x,y) = E_L(x,y) + D_L(x,y) \tag{14}$$

where, $C_L(x,y)$ is the low-frequency coefficient value of the subgraph, $\omega(i,j)$ is the weight, and the correlation value calculated by the window with 3×3 in the text. The weight value is:

$$\omega = \frac{1}{15} \times \begin{bmatrix} 1 & 2 & 1 \\ 2 & 3 & 2 \\ 1 & 2 & 1 \end{bmatrix} \tag{15}$$

Then the similarity of the low frequency subgraphs of the two source images in the same area is:

$$S(i,j) = \frac{M_L^A(x,y)}{M_L^A(x,y) + M_L^B(x,y)} \tag{16}$$

The threshold is selected as $T = 0.55$. In order to increase the robustness of the algorithm, let $\alpha = T/(1+T)$, $\beta = 1/(1+T)$. If the similarity value is greater than α or equal to 1\2 or greater than 1\2 and less than or equal to β, the similarity between the two subgraphs is higher. Subgraph fusion is performed by weighted fusion for two subgraphs:

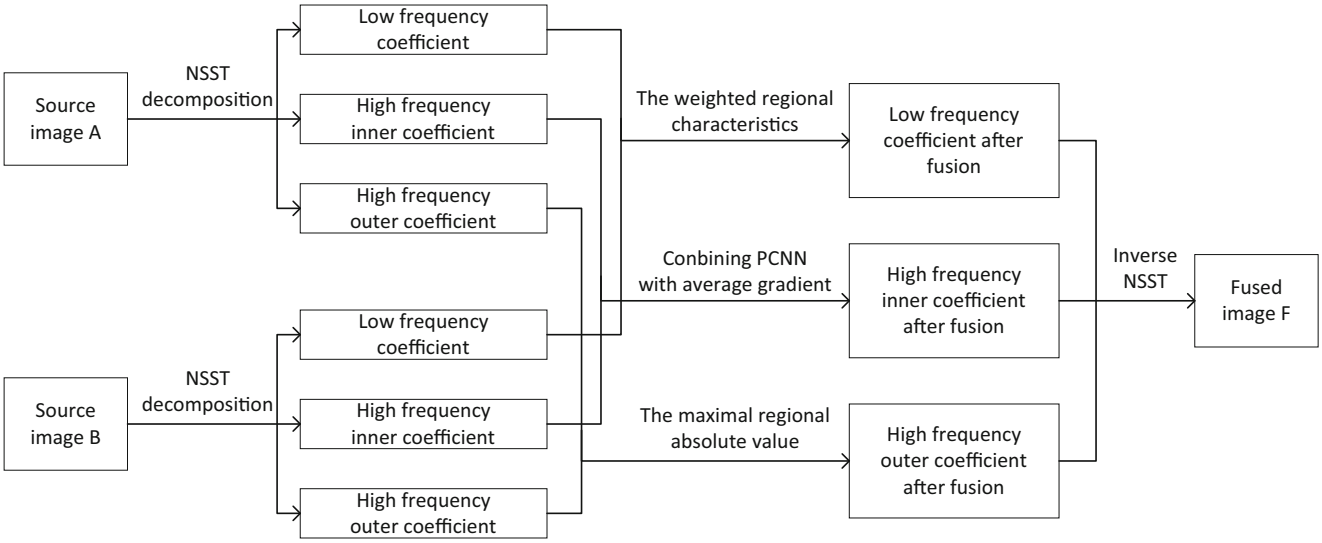

Fig. 2 Flow chart of the proposed algorithm in the paper

$$C_L^F = a(i,j)C_L^A(x,y) + (1-a(i,j))C_L^B(x,y) \tag{17}$$

Where the weight $a(i,j)$ is calculated as:

$$a(i,j) = \begin{cases} 0.5-0.5\left[\dfrac{1-2s(i,j)}{1-2\alpha}\right], s(i,j)\in(\alpha, 0.5) \\ 0.5+0.5\left[\dfrac{1-2s(i,j)}{1-2\alpha}\right], s(i,j)\in(0.5, \beta) \end{cases} \tag{18}$$

2.3.2 Low similarity low frequency subgraph fusion

The Pulse Coupled Neural Network (PCNN) model is a simplified new neural network model established by simulating the phenomenon of synchronous pulse release in the cat's visual cortex [17]. PCNN is widely used However, the PCNN model is similar to the actual biological brain neural network operation mechanism, although there are many improved algorithms, the accurate setting of a large number of parameters and iterations and the reduction of computational complexity are still not effectively solved [21]. To this end, an algorithm for the fusion of dissimilar subgraphs using the improved connection term of Linking Synaptic Computation Network (LSCN) is proposed. The model structure of the algorithm is simplified, the number of parameters to be determined is greatly reduced, the computational complexity is reduced, and the problem that it is difficult to determine the number of iterations in the multi-channel working mode is solved.

In the LSCN model, the pixels in the image are equivalent to the neurons. When a neuron is present, the neuron fires a pulse. At this point the threshold is rapidly increased

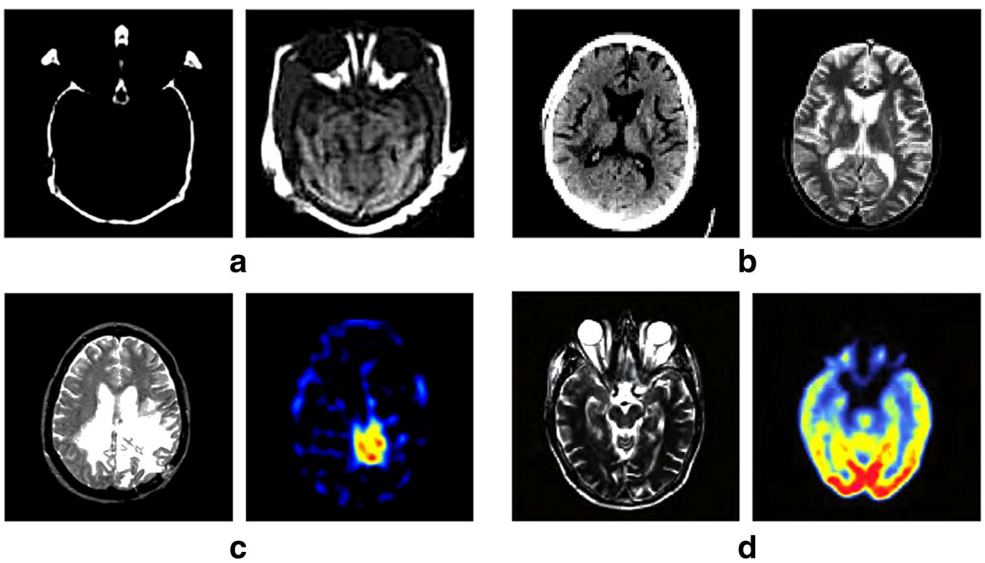

Fig. 3 Representative of 4 sets of image data used in experiments. (**a**) The first set of experimental images (**b**) The second set of experimental (**c**) The third set of experimental images (**d**) The fourth set of experimental

according to the feedback input, causing the neuron to stop transmitting pulses [22]. The fusion of indicators in image fusion directly affects the fusion results. In the previous fusion algorithm based on PCNN and its improved model, the pixels of the fused image are determined according to the firing frequency of the neurons after several iterations [23]. The ignition frequency is calculated by the L-term (formula 2) of the LSCN network, and the L-term is convoluted for each output pulse to make the output better.The characteristics of the image are usually determined by the pixels of a certain area. Considering the influence of noise and the interaction between the neighborhoods of pixels, a single L term will reduce the quality of the fused image. For this reason, the binder Figure similarity judgment, using region enhancement L term for fusion, ie

$$E_L^J(x,y) = \overline{T}_L^J(x,y) \times e^{b \times s_L^J(x,y)} \tag{19}$$

Where, $b \in [-10, 10]$ is the adjustment factor which is used to weigh the importance of the mean and standard deviation in the neighborhood $M \times N$, $\overline{T}_L^J(x,y)$ and $s_L^J(x,y)$ are the mean and standard deviation of the fire map in the neighborhood, the neighborhood still selects the window as 3×3, then

$$\overline{T}_L^J(x,y) = \frac{1}{M \times N} \cdot \sum_{i=-\frac{M-1}{2}}^{i=\frac{M-1}{2}} \sum_{j=-\frac{N-1}{2}}^{j=\frac{N-1}{2}} T_L^J(x+i, y+j) \tag{20}$$

$$s_L^J(x,y) = \sqrt{\sum_{i=-\frac{M-1}{2}}^{i=\frac{M-1}{2}} \sum_{j=-\frac{N-1}{2}}^{j=\frac{N-1}{2}} \left(\overline{T}_L^J(x+i, y+j) - T_L^J(x,y) \right)^2} \tag{21}$$

where, $T_L^J(x,y)$ is the number of firings of the pixel in the position. In the LSCN stacking process, in order to avoid the unreasonable setting of the maximum number of iterations, when all the neurons are ignited, the iteration is terminated [7]. The strategy of low-frequency subgraph fusion with low similarity is:

$$C_L^F = \begin{cases} C_L^A(x,y), E_L^A(i,j) > E_L^B(i,j) \\ C_L^B(x,y), E_L^A(i,j) < E_L^B(i,j) \end{cases} \tag{22}$$

2.4 Frequency modulation image fusion

The high frequency sub-image can reflect details such as the texture or edge of the source image. In these detail regions, the sub-band coefficient values fluctuate greatly, and the visual system is sensitive to these characteristic regions [24]. Therefore, firstly, the structural similarity of the subgraph is still judged, and the subgraph with high similarity indicates that the structural contour is similar, the correlation is strong, and the strategy of weighted integration is adopted; subgraphs with low similarity indicate that the image structure features are different. Features are fused through an improved guided filtering algorithm.

2.4.1 Subgraph fusion with high similarity

The image area has a high degree of similarity, reflecting the fact that the two images have similar texture details in the area. If a weighted fusion rule is used, the image-specific texture features are weakened [25]. This paper combines the visual sensitivity coefficient with the regional energy, namely

$$C_L^F = \begin{cases} C_L^A(x,y), \left(e^{E_A^J(x,y)} + e^{vsc_A^J(x,y)} \right) > \left(e^{E_B^J(x,y)} + e^{vsc_B^J(x,y)} \right) \\ C_L^B(x,y), \left(e^{E_A^J(x,y)} + e^{vsc_A^J(x,y)} \right) > \left(e^{E_B^J(x,y)} + e^{vsc_B^J(x,y)} \right) \end{cases} \tag{23}$$

where, $E_L^J(x,y)$ Energy value in the neighborhood $M \times N$, $vs\ c_L^J(x,y)$ is the visual sensitivity coefficient,

$$E_L^J(x,y) = \frac{1}{M \times N} \cdot \sum_{i=-\frac{M-1}{2}}^{i=\frac{M-1}{2}} \sum_{j=-\frac{N-1}{2}}^{j=\frac{N-1}{2}} \left(\omega(i,j) \cdot C^2(x+i, y+j) \right) \tag{24}$$

$$vsc_L^J(x,y) = \left| \frac{C_L^J(x,y)}{\overline{C}_L^J(x,y)} \right| \tag{25}$$

where, $\omega(i,j)$ is the weight。.

2.4.2 Subgraph fusion with low similarity

For low mutual sub-band images, the same area contains important information and the difference is large; when performing coefficient fusion, it is necessary to consider the interaction between the high and low frequency sub-bands and the image clarity [26]. Fusion is performed using improved pilot filtering. Phase consistency means that the frequency of the edge features in the image frequency domain is higher at the same stage, and the edge information can be detected without being affected by the change of the local light brightness of the image, and can be well preserved at the edge with low contrast of the image. Edge information. The weighting factor $\psi(i)$ based on phase consistency is used instead of the weighting factor ε in Eq. (8).

$$\psi(i) = \frac{1}{M \times N} \sum_{k=1}^{M \times N} \frac{|P_c(i)|}{|P_c(k)| + \gamma} \tag{26}$$

where, γ is used to prevent the denominator from appearing a small number of zero values, $P_c(i)$ is the phase consistency calculation for the two-dimensional image

$$P_c(x) = \frac{\sum_n W(x)[A_n(x)\Delta\varphi_n(x) - T]}{\sum_n [A_n(x)\Delta\varphi_n(x) + \lambda]} \tag{27}$$

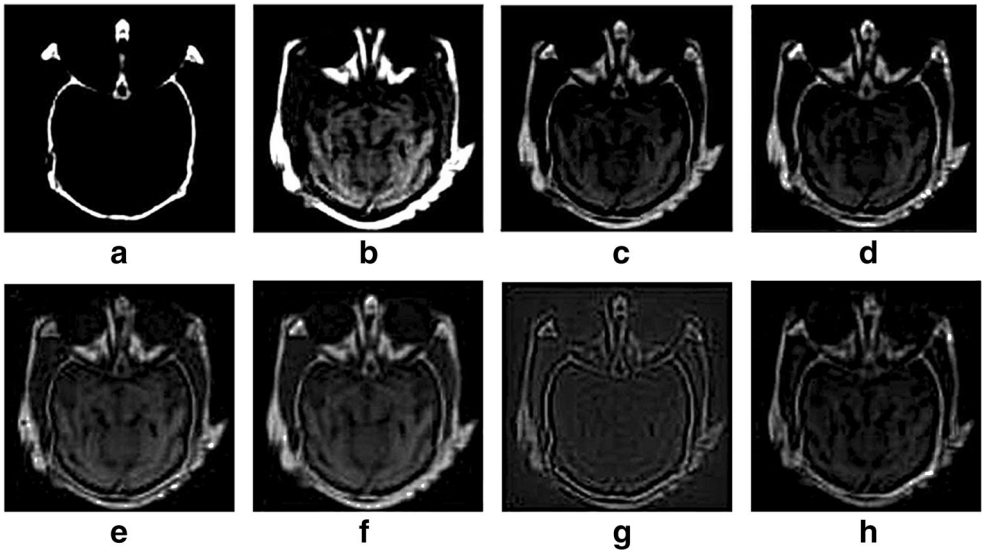

Fig. 4 Experiment results of Normal brain CT-MRI medical image fusion results on the first group. (**a**) CT source image (**b**) MRI source image (**c**) DWT algorithm (**d**) CLT algorithm (**e**) NSST-RP algorithm (**f**) NSCT-IGF algorithm (**g**) LSCN-L algorithm (**h**) NSST-imL algorithm

Where, T is the noise value, $W(x)$ is the frequency weight, and λ is the same as γ . Laplacian filtering L_p is performed on the subgraph and a high-pass image $H^u_{i,k}$ is obtained. Average filtering A_{avg} is performed to obtain a saliency map $S^u_{i,k}$:

$$S^u_{i,k} = ||C^u_{lk}(x,y) - C^u_{lk}(x,y) \cdot L_p| \cdot A_{avg}| \tag{28}$$

Where, $C^u_{lk}(x,y)$ is the transform coefficient value after the NSST is performed on the source image in the first direction k on the scale l.

Guided filtered image $p^u_{i,k}$ can be calculated from the significant map:

$$P^u_{lk}(x,y) = \begin{cases} 1, S^u_{lk} = \max\left(S^A_{lk}, S^B_{lk}\right) \\ 0, \quad \text{otherwise} \end{cases} \tag{29}$$

The high-frequency subgraph fusion strategy for obtaining similarity is:

$$C^F_L = \begin{cases} C^A_L(x,y), P^A_{lk} > P^B_{lk} \\ C^B_L(x,y), P^A_{lk} \le P^B_{lk} \end{cases} \tag{30}$$

3 Experimental results and analysis

In order to verify the performance of the medical image algorithm proposed in this paper, four sets of source image pairs of Harvard Medical School were used for experimental verification. The first and second groups are the registered CT-MRI grayscale images of the head. The CT images are clearly visible to high-density tissues (such as bones), but not good for low-density soft tissues. MRI imaging is opposite to CT. The CT-MRI fusion can make up for their shortcomings. The two images are from the normal brain and brain toxoplasmosis

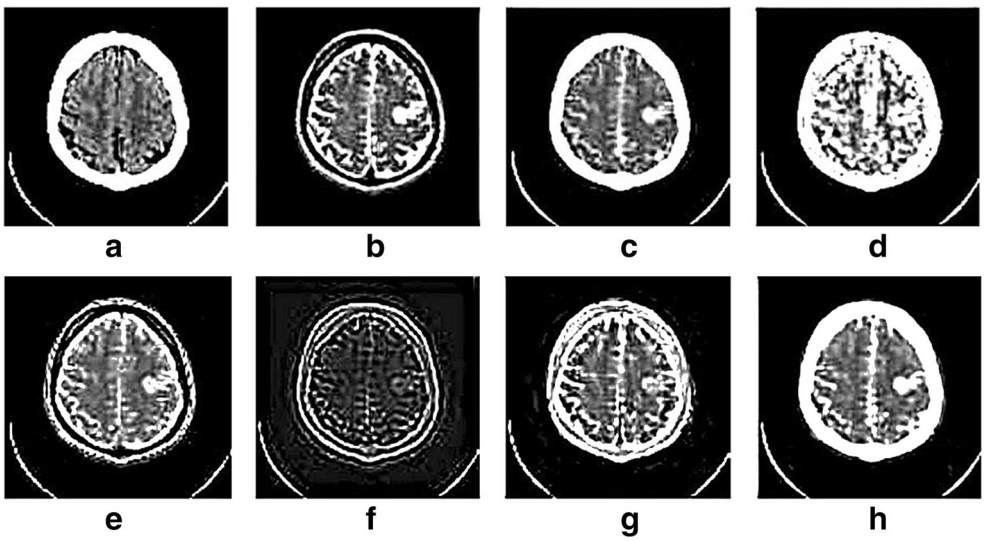

Fig. 5 Fusion Results of CT-MRI image with cerebral toxoplasmosis in the second group. (**a**) CT source image (**b**) MRI source image (**c**) DWT algorithm (**d**) CLT algorithm (**e**) NSST-RP algorithm (**f**) NSCT-IGF algorithm (**g**) LSCN-L algorithm (**h**) NSST-imL algorithm

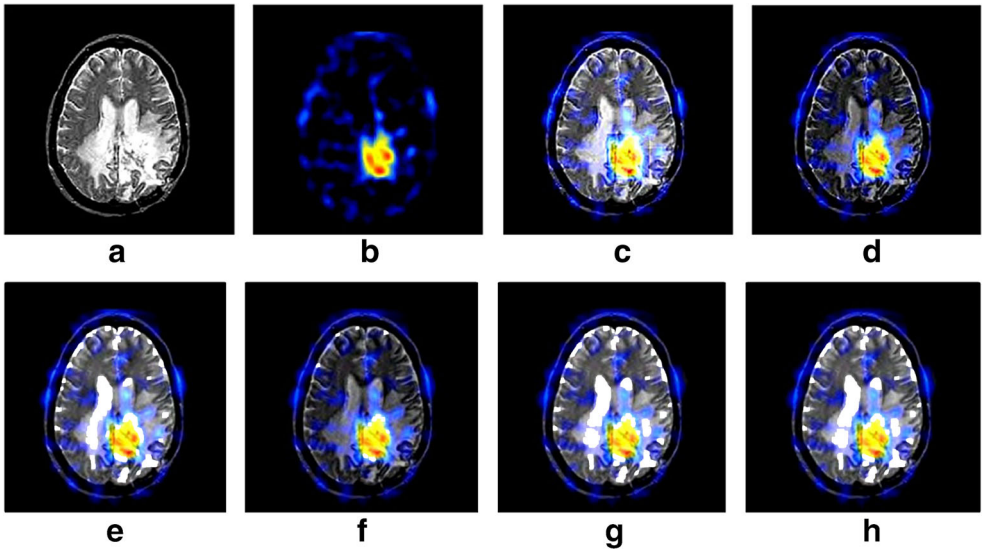

Fig. 6 Fusion results of the MRI-SPECT images in the third group. (**a**) CT source image (**b**) MRI source image (**c**) DWT algorithm (**d**) CLT algorithm (**e**) NSST-RP algorithm (**f**) NSCT-IGF algorithm (**g**) LSCN-L algorithm (**h**) NSST-imL algorithm

brain. The third group was an MRI-SPECT source image from a 51-year-old woman with progressive astrocytoma, and the fourth group was an MRI-PET source image. Each of the four groups of images has 50 images. The four groups of images are shown in the figure, and each image has a pixel size of 256 × 256. Due to space limitations, only a pair of representative images in each set of experimental data are shown in Fig. 3.

Five classic medical image fusion algorithms are selected to participate in performance comparison experiments, that is DWT [7], CLT [8], NSST-RP [12], NSCT-IGF [18] and LSCN-L [27]. The literature based on lifting wavelet transform proposed in [7], using regional energy weighting rules for low frequency sub-bands, and fused image of fusion rules of box-box fractal method and region gradient for high-frequency sub-bands of different noises (abbreviated as DWT). The medical image fusion method based on contourlet transform coefficient weighting proposed in [8], the low-frequency coefficients adopt the regional variance weighted fusion rule, and the high-frequency sub-band coefficients adopt the conditional weighted fusion rule (abbreviated as CLT). Fusion image based on NSST and regional ignition PCNN medical image fusion method proposed in [12] (abbreviated as NSST-RP). Combining NSCT with Improved Guided Filtering Algorithm (NSCT-IGF) in [18]. Multi-focus image fusion algorithm based on L-term of single-frequency LSCN algorithm proposed in [25] as fusion strategy (abbreviation LSCN-L). NSST-imL is an abbreviation of the algorithm proposed in this paper.

3.1 Visual effect comparison experiment

What has been shown from Figs. 4, 5 and 6 is the fusion results of the five comparison algorithms and the proposed algorithm in

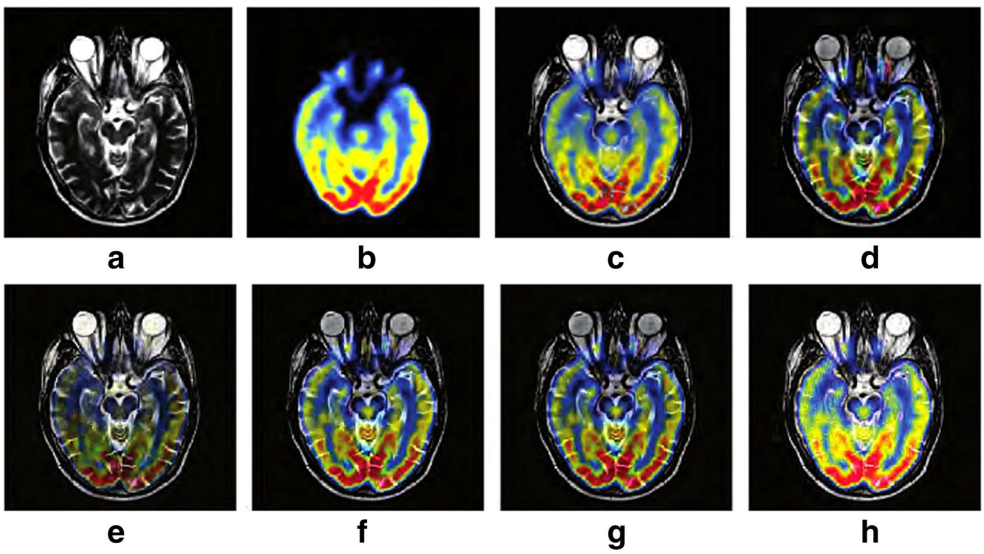

Fig. 7 Fusion results of the MRI-PET images in the fourth group. (**a**) CT source image (**b**) MRI source image (**c**) DWT algorithm (**d**) CLT algorithm (**e**) NSST-RP algorithm (**f**) NSCT-IGF algorithm (**g**) LSCN-L algorithm (**h**) NSST-imL algorithm

the four sets of experimental medical images. Only one comparison result is listed for each experimental image.

It can be seen from the results of the image fusion experiment shown in the figure that the six algorithms successfully combine the two images together, and can simultaneously highlight the bone part and soft tissue information of the brain, and the effect is good.Further analysis reveals that, the visual effects in Figs. 4c and 4d are similar, but some of the information in the source MRI is lost, the soft tissue and bone information images in Fig. 4e are not ideal,the fusion results of Fig. 4f-h are better, but Fig. 4h has a good visual effect, and the spatial detail information of the image is well preserved, and the imaging quality is the best.

It can be seen from the MRI image of patients with cerebral toxoplasmosis in Fig. 5. The details in Fig. 5c and d are rich, but the image is dark and difficult to observe. Many details in the source MRI in Fig. 5e are weakened. Figure 5f, g, and h are superior in visual effects to other comparison algorithms, but the information-rich imaging quality is best in this algorithm.

In Fig. 6 and Fig. 7, Figure (c) and (d) perform poorly on the extraction and expression of SPECT source image information, and there are some artifacts. Figure (e) The visual effect is relatively better, but the same problem exists. In contrast, the sharpness and contrast of graphs (f), (g), and (h) are higher, but the soft tissue part of the algorithm is closer to the source image, and the fusion effect is the best.

It is found that the poor ability of wavelet to represent high-dimensional feature information leads to the obvious obstructive effect of the wave transform (shown by the red arrow in the figure), and many related parameters are set unreasonably, resulting in the fusion image obtained by the contour wave and the ordinary shear wave method. The image contrast is low.Compared with the image fusion based on NSST decomposition, the proposed algorithm has a clearer edge contour than the region-based ignition PCNN and single-pixel L-item fusion strategy. The contrast is higher, the image texture is basically consistent with the source image, and the visual effect is more obvious.

Table 1 Quality evaluation of medical fusion images generated by different algorithms in Fig. 4

Fused image	Evaluation index						
	MI	*SD*	$Q^{AB/F}$	*IE*	*SF*	*AG*	*SSIM*
c	4.136	41.378	0.718	5.995	11.182	7.295	0.515
d	3.212	40.266	0.592	6.078	10.975	7.539	0.496
e	3.698	36.017	0.711	5.769	9.765	4.826	0.531
f	1.476	22.981	0.525	5.216	9.270	7.328	0.317
g	1.938	30.631	0.546	5.459	8.216	6.553	.0425
h	4.398	45.173	0.785	6.072	11.976	7.319	0.578

Table 2 Quality evaluation of medical fusion images generated by different algorithms in Fig. 4

Fused image	Evaluation index						
	MI	*SD*	$Q^{AB/F}$	*IE*	*SF*	*AG*	*SSIM*
c	3.529	49.821	0.708	6.736	11.079	7.936	0.736
d	3.015	38.134	0.519	7.011	10.946	8.012	0.701
e	3.238	35.261	0.698	6.329	10.215	5.615	0.798
f	1.052	40.102	0.476	5.974	10.198	7.635	0.651
g	1.633	41.226	0.503	5.336	9.875	7.021	0.679
h	3.796	51.325	0.729	7.021	11.851	8.326	0.815

3.2 Performance comparison experiment

In order to evaluate the fusion results more comprehensively, based on the subjective visual evaluation of human eyes, seven objective evaluation indicators such as mutual information and standard deviationMutual Information (MI), Standard Deviation (SD), Edge Information Evaluation Factor ($Q^{AB/F}$), Information Entropy (IE), Spatial Frequency (SF), Average Grads (AG), and Structural Similarity (SSIM) are selected to evaluate the fusion quality of images. The evaluation results are shown in Tables 1, 2, 3 and 4. The data in the table is the average value after the correlation of all the images in each group. The larger the value of the indicator in the table, the more accurate the information in the image after fusion, the better the fusion effect.

It can be seen from the experimental results that the algorithm fusion effect of the fusion image with the ignition frequency as the index has achieved good experimental results on all indicators. In this paper, the region L term is selected as the output, which is higher than the single pixel in each evaluation index. L term and region PCNN ignition frequency as output value. Compared with the wavelet and contour wave methods, the algorithm can maximize the mutual information and entropy in the case of translation invariance, indicating

Table 3 Quality evaluation of medical fusion images generated by different algorithms in Fig. 4

Fused image	Evaluation index						
	MI	*SD*	$Q^{AB/F}$	*IE*	*SF*	*AG*	*SSIM*
c	2.261	31.628	0.710	4.125	33.421	6.362	0.596
d	2.412	30.126	0.523	4.210	34.356	7.215	0.651
e	2.835	26.017	0.706	4.632	36.791	5.331	0.763
f	2.701	22.198	0.518	4.481	34.872	6.473	0.755
g	2.852	25.331	0.525	4.702	37.956	6.511	0.787
h	3.083	32.112	0.751	4.765	39.551	7.325	0.875

Table 4 Quality evaluation of medical fusion images generated by different algorithms in Fig. 4

Fused image	Evaluation index						
	MI	*SD*	$Q^{AB/F}$	*IE*	*SF*	*AG*	*SSIM*
c	5.235	35.729	0.342	6.021	39.407	5.394	0.628
d	4.972	34.663	0.359	6.325	40.215	6.219	0.701
e	6.026	32.215	0.321	5.469	42.372	4.982	0.715
f	4.759	29.841	0.365	4.982	40.451	5.321	0.694
g	4.588	31.095	0.356	5.757	43.211	5.401	0.573
h	6.262	35.971	0.369	6.196	45.109	6.370	0.735

that NSST can provide a better sparse representation of the fused image, and the fusion result is more realistic. The spatial frequency and standard deviation can be maximized to indicate that the fusion results are better in terms of contrast and brightness. The highest MI and SSIM index values indicate that the edge information between the fused image and the source image is the best; considering the amplitude characteristics and phase distribution information of the coefficients, the image structure information is better, the spatial detail information and structural information are richer, and the visual effect is better.

From the overall experimental results, the proposed algorithm can get better fusion performance in edge detail definition, gray level change and color contrast, and the objective evaluation is consistent with the visual observation result, and thus, The effectiveness of the proposed algorithm and be verified.

4 Conclusion

Multimodal medical image fusion organically combines source image information so that doctors can understand the comprehensive organization of diseased tissues or organs.

In view of the situation, and to make a more accurate diagnosis or to develop a more appropriate treatment plan, a medical image fusion algorithm based on NSST frequency division and improved LSCN is proposed. Based on the NSST frequency-dividing and similarity evaluation, the weighted fusion method is adopted for the sub-images with high similarity, and then, the improved L-sub-field for LSCN is used for image fusion for the low-frequency sub-pictures with low similarity, and the improved guided filtering strategy is used for image fusion for the high frequency subgraph with low similarity to high frequency, the edge and detail information of the source image is more complete and realistic. The experimental results show that the proposed algorithm can obtain better fusion effects in both objective and subjective evaluation. The obtained fusion image has rich information, excellent edge retention characteristics, subjectively clear texture and high contrast and good visual effect. Compared with the traditional fusion algorithm, this paper needs to further study the optimization of related parameter settings. Theoretical analysis and experimental results show that the proposed algorithm is simple and easy to implement, not only reduces the number of parameters to be determined, reduces the computational complexity, but also solves the problem that the number of iterations in traditional models is difficult to determine; the algorithm not only performs well in subjective aspects; It is better than the comparison algorithm in edge information evaluation factor, information entropy, standard deviation, spatial frequency and sharpness.

References

1. Zhao W, Lu H (2017) Medical image fusion and Denoising with alternating sequential filter and adaptive fractional order Total variation[J]. IEEE Trans Instrum Meas 66(9):2283–2294
2. Du J, Li W, Xiao B (2017) Anatomical-functional image fusion by information of interest in local Laplacian filtering domain.[J]. IEEE Trans Image Process A Publication of the IEEE Signal Process Soc 12(60):5855–5866
3. Manchanda M, Sharma R (2018) An improved multimodal medical image fusion algorithm based on fuzzy transform[J]. J Vis Commun Image Represent 51:76–94
4. Villadsen J, Hansen HD, Jørgensen LM, Keller SH, Andersen FL, Petersen IN, Knudsen GM, Svarer C (2018) Automatic delineation of brain regions on MRI and PET images from the pig.[J]. J Neurosci Methods 294:51–58
5. Soundrapandiyan R (2017) An efficient DWT and intuitionistic fuzzy based multimodality medical image fusion[J]. Int J Imaging Syst Technol 27(2):118–132
6. Huang Z, Ding M, Zhang X (2017) Medical image fusion based on non-subsampled Shearlet transform and spiking cortical model[J]. J Med Imaging Health Inform 7(1):229–234
7. Jun-feng L, Xiao-li J, Wen-zhan D (2014) Medical image fusion based on lifting wavelet transform[J]. J Image Graph 19(11):1639–1648 (in Chinese)
8. Vishwakarma A, Bhuyan MK, Iwahori Y (2018) Non-subsampled shearlet transform-based image fusion using modified weighted saliency and local difference[J]. Multimed Tools Appl 77(21):1–28
9. Huang Y, Bi D, Wu D (2018) Infrared and visible image fusion based on different constraints in the non-subsampled Shearlet transform domain.[J]. Sensors 18(4):1169–1181
10. Ouerghi H, Mourali O, Zagrouba E (2018) Non-subsampled shearlet transform based MRI and PET brain image fusion using simplified pulse coupled neural network and weight local features in YIQ colour space[J]. IET Image Process 12(10):1873–1880
11. Bhateja V, Moin A, Srivastava A et al (2016) Multispectral medical image fusion in Contourlet domain for computer based diagnosis of Alzheimer's disease[J]. Rev Sci Instrum 87(7):1–7
12. Ganasala P, Kumar V (2016) Feature-motivated simplified adaptive PCNN-based medical image fusion algorithm in NSST domain[J]. J Digit Imaging 29(1):73–85
13. Cheng B, Jin L, Li G (2018) A novel fusion framework of visible light and infrared images based on singular value decomposition

and adaptive DUAL-PCNN in NSST domain[J]. Infrared Phys Technol 16(9):37–45
14. ZHAO D, DAI WZ, LI J F. (2018) Medical image fusion based on NSST and improved PCNN[J]. J Optoelectron Laser 29(1):95–104
15. He K, Sun J, Tang X (2013) Guided image filtering[J]. IEEE Trans Pattern Anal Mach Intell 35(6):1397–1409
16. Li S, Kang X, Hu J (2013) Image fusion with guided filtering[J]. IEEE Trans Image Process 22(7):2864–2875
17. Zhu D, Xu L, Wang FB et al (2018) Multi-focus image fusion algorithm based on fast finite Shearlet Transformand guided filter[J]. Laser & Optoelectron Prog 55(1):196–203 (in Chinese)
18. Wang RR, Yang YD (2018) Image fusion algorithm based on complex Shearlet transform coupled with improved guided filtering[J]. J Electron Meas Instrum 5:126–133
19. Sun G, Li J, Dai J et al (2018) Feature selection for IoT based on maximal information coefficient[J]. Futur Gen Comput Syst The Int J Esci 89:606–616
20. Sun G, Chen T, Su Y et al (2018) Internet traffic classification based on incremental support vector machines[J]. Futur Gen Comput Syst The Int J Esci 23(4): 789–796
21. Bavirisetti DP, Kollu V, Gang X, Dhuli R (2017) Fusion of MRI and CT images using guided image filter and image statistics[J]. Int J Imaging Syst Technol 27(3):227–237
22. ZHAN K, SHI JH, TENG JC et al (2017) Linking synaptic computation for image enhancement [J]. Neurocomputing 238:1–12
23. Wang ZB, Ma YD, Gu J (2010) Multi- focus image fusion using PCNN[J]. Pattern Recogn 43(6):2003–2016
24. Deng XY, Ma YD, Dong M (2016) A new adaptive filtering method for removing salt and pepper noise based on multilayered PCNN[J]. Pattern Recogn Lett 79:8–17
25. Wang Z, Shuai W, Ying Z (2017) Multi-focus image fusion based on the improved PCNN and guided filter[J]. Neural Process Lett 45(1):75–94
26. He F, Guo Y, Chao G (2017) Human segmentation of infrared image for mobile robot search[J]. Multimed Tools Appl 12:1–14
27. Cheng B, Jin L, Li G (2018) Adaptive fusion framework of infrared and visual image using saliency detection and improved dual-channel PCNN in the LNSST domain[J]. Infrared Phys Technol 92:30–43